New Journal of Physics
The open-access journal for physics

State-dependent, addressable subwavelength lattices with cold atoms

W Yi[1], **A J Daley, G Pupillo and P Zoller**
Institute for Quantum Optics and Quantum Information of the Austrian Academy of Sciences, A-6020 Innsbruck, Austria
and
Institute for Theoretical Physics, University of Innsbruck, A-6020 Innsbruck, Austria
E-mail: wei.yi@uibk.ac.at

New Journal of Physics **10** (2008) 073015 (22pp)
Received 28 April 2008
Published 8 July 2008
Online at http://www.njp.org/
doi:10.1088/1367-2630/10/7/073015

Abstract. We discuss how adiabatic potentials can be used to create addressable lattices on a subwavelength scale, which can be used as a tool for local operations and readout within a lattice substructure, while taking advantage of the faster timescales and higher energy and temperature scales determined by the shorter lattice spacing. For alkaline-earth-like atoms with nonzero nuclear spin, these potentials can be made state-dependent, for which we give specific examples with ^{171}Yb atoms. We discuss in detail the limitations in generating the lattice potentials, in particular non-adiabatic losses, and show that the loss rates can always be made exponentially small by increasing the laser power.

[1] Author to whom any correspondence should be addressed.

Contents

1. Introduction

Optical lattices in three dimensions (3D) generated by counterpropagating laser fields provide a periodic array of microtraps for cold atoms, and implement quantum lattice models governed by Hubbard Hamiltonians [1]. This is of interest both in the study of strongly correlated systems from condensed matter physics, and in the implementation of quantum information processing. Two key elements of cold atom dynamics in 3D optical lattices are: (i) the lattice spacing is bounded below by the wavelength $a \equiv \lambda/2$. Therefore, all the relevant time, energy and temperature scales are determined by the recoil energy, $E_R = \hbar^2 k^2/(2m)$, where $k = 2\pi/\lambda$ is the wavenumber, and m is the mass of the atom. In particular, the hopping matrix element between neighbouring sites within the region of validity of the single-band Hubbard model is limited by $J \ll E_R$. This limits all corresponding timescales, for example the timescale over which entanglement can be generated using exchange interactions [2, 3]. (ii) Varying the laser parameters provides *global* control of the lattice potential, but development of tools for local operations and readout remains a major challenge in light of applications in quantum computing and quantum simulation [4]. Here, we show how adiabatic potentials can be used to address these issues by creating addressable, state-dependent subwavelength lattices. Each lattice period can be divided into a set of wells, which can be frequency addressed via their offset energies, reminiscent of quantum computing schemes with electrons in arrays of electrically gated quantum dots [5].

In recent seminal experiments [2, 3], optical superlattices have been used to provide addressability and to entangle atoms in a series of double-wells in one parallel operation. Our goal here is to achieve similar control on subwavelength scales by coupling optical lattice potentials with dressing fields, with the benefit that all corresponding timescales are significantly

faster, and energy and temperature scales significantly higher. Single particle effects of such dressed potentials [6]–[14] have been studied, e.g. in the context of lithography [15], laser cooling [16, 17] and radio frequency (RF)-dressed potentials on atom chips [18]. Here, we show how the adiabatic potentials, created by coupling optical lattice potentials with additional dressing fields, can be used for subwavelength control in the context of manybody physics. We will demonstrate how adiabatic potentials can be used to generate state-dependent, addressable subwavelength lattices. In such a subwavelength lattice, each lattice period is subdivided into several potential wells, for which the relative well depth can be tuned by either applying external magnetic or electric fields, or by adjusting the laser parameters, e.g. the Rabi frequency and detuning. Atoms loaded into different wells within the subwavelength structure can also be frequency addressed via their different offset energies.

In view of recent seminal progress with alkaline-earth-like atoms, e.g. in the context of developing optical clocks [19, 20], in many-body cold atom physics [21] and in applications in quantum information [22, 23], we investigate, in particular, the possibility for generating subwavelength potentials with these species. The existence of metastable triplet states makes possible the production of near-resonant optical lattices, which allow for the creation of state-dependent subwavelength lattices. We show how this can be used to generate and manipulate entanglement, making use of the spin dependence and/or shorter tunnelling times within the subwavelength structure. Of course, in the context of adiabatic potentials, the question of non-adiabatic losses will always arise. We analyse these losses in detail in the present context, and conclude that they can always be suppressed at the expense of using additional laser power.

This paper is organized as follows: we first give a general description in section 2 of two schemes to create adiabatic potentials with two-level atoms. In section 3, we extend the idea to multi-level atoms, describing the additional control that is present when these lattices are generated for real atoms. In particular, we discuss possibilities for state-dependent potentials with alkaline-earth-like atoms. In section 4, we add interactions between atoms and give examples for possible applications of subwavelength lattices in quantum simulation and quantum information. This includes a discussion of how entanglement within the subwavelength structure can be generated and controlled. In section 5, we analyse the Landau–Zener-type loss rate from the adiabatic potentials in detail and discuss how it should be suppressed. In the appendix, we give additional details on the clock transition in alkaline-earth-like atoms, which are essential for the generation of subwavelength lattices with these atoms.

2. Generating subwavelength lattice potentials

In this section, we introduce the basic ideas behind addressable subwavelength potentials for two-level atoms. This will be generalized to multi-level atoms in section 3, where we also discuss their implementation with alkaline-earth-like and alkali atoms, and how they can be made internal state- (or qubit-) dependent. We discuss these ideas on the single-particle level initially, with interactions between atoms to be added in section 4.

As shown in figure 1(a), our goal is to divide each period of a standard $\lambda/2$ optical lattice into several potential wells with controllable barrier heights and well depths in this subwavelength structure. A laser can then be used to address atoms on different sites independently based on energy selectivity, coupling to an unperturbed reference state. In addition, we can control in this way the tunnelling of atoms between adjacent wells in the subwavelength structure.

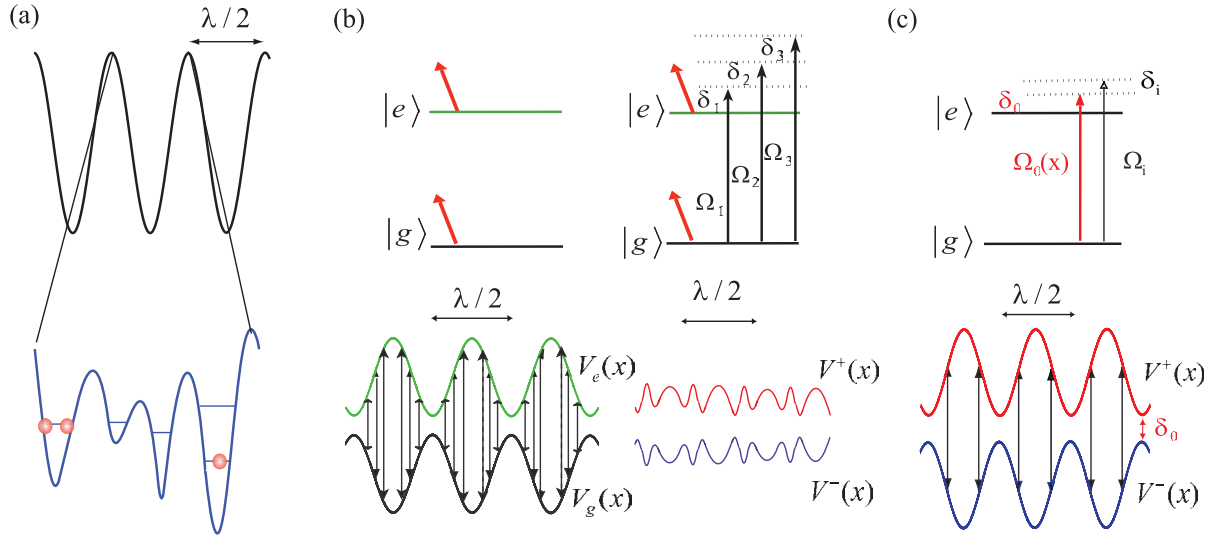

Figure 1. Subwavelength lattice with off-resonant and near-resonant $\lambda/2$ background potentials (see text). (a) Schematic of a controllable subwavelength lattice, where each lattice period of an initial $\lambda/2$ is subdivided into several potential wells whose position and well depth can be controlled by changing the laser parameters. Note that addressability in the subwavelength lattice is modulo $\lambda/2$, with λ the wavelength of the laser generating the background lattice potentials. (b) (left) Level structure and laser configurations for generating background potentials $V_{g,e}(x)$ in the off-resonant scheme. (right) Dressing fields with the Rabi frequency Ω_i $(i = 1, 2, 3, \ldots)$ and detuning δ_i are applied to couple the background potentials to generate sub-wavelength lattice $V^{\pm}(x)$. The separation between neighbouring wells is approximately $\lambda/2(n+1)$ with n dressing fields. (c) Level structure and laser configurations for generating near-resonant sub-wavelength potentials in a two level system. The counteroscillating background potentials $V^{\pm}(x)$ are now induced by directly coupling the two levels $|g\rangle$ and $|e\rangle$ with standing wave fields with the Rabi frequency $\Omega_0(x)$ and detuning δ_0 (red). Dressing fields with the Rabi frequency Ω_i $(i = 1, 2, \ldots)$ couple the background potentials to generate the subwavelength potential.

The simplest way to achieve this goal is shown in figure 1(b). We consider a two-level atom with two long-lived internal states $|e\rangle$ and $|g\rangle$. We assume that we can generate counter-oscillating *off-resonant* potentials for these two internal states, for which the implementation will be discussed in section 3. We then couple the internal states with additional dressing fields, which generate avoided crossings in the background potentials, and thus a subwavelength structure. Here, the well depth and barrier heights can be controlled by varying the detunings and Rabi frequencies of the dressing fields, which shifts the locations of the avoided crossings. In figure 1(b), we show the simplest case with isolated avoided crossings.

It is also possible to generate background potentials with *near-resonant* coupling between $|g\rangle$ and $|e\rangle$ with a Rabi frequency varying sinusoidally in space (e.g. as generated by a standing wave light field). This results in counter-oscillating potentials due to ac-Stark splitting, which can then be coupled by a series of dressing fields to produce the desired subwavelength

structure (see figure 1(c)). This scheme is motivated, in particular, by alkaline-earth-like atoms (as discussed in section 3).

2.1. Addressable subwavelength lattices with two-level atoms in 1D: off-resonant scheme

We now discuss the details of the generation of subwavelength lattices with off-resonant background potentials for a two-level atom. In the rotating wave approximation with respect to the optical frequencies, we may write the single atom Hamiltonian as:

$$H = H_M + H_0 + H_1, \tag{1}$$

with

$$\begin{aligned} H_M &= \frac{\hat{p}^2}{2m}, \\ H_0 &= V_g(x)|g\rangle\langle g| + (V_e(x) - \delta_1)|e\rangle\langle e| \\ H_1 &= \sum_{n=1,2,\ldots} \frac{\Omega_n}{2} \exp(-\mathrm{i}(n-1)\delta t)|e\rangle\langle g| + \mathrm{h.c.} \end{aligned} \tag{2}$$

Here, H_M is the kinetic energy, H_0 describes the background potentials and H_1 contains the dressing fields with Rabi frequencies Ω_n. For dressing fields produced as an equally-spaced comb of sidebands, the detunings can be written as $\delta_n = \delta_1 + (n-1)\delta$, where δ_1 is the detuning of the first dressing field. In the off-resonant scheme, the background potentials for the two internal states are generated by standing wave fields and are opposite to one another. For this, we may take $V_g(x) = -V_e(x) = -V_0 \sin^2(kx)$, where $k = 2\pi/\lambda$ is the wavenumber of the laser generating the background potential.

Generation of the adiabatic potentials is based on the validity of a Born–Oppenheimer-type assumption. This involves the fact that the kinetic energy of the atoms is small on a scale given by the separation of the resulting adiabatic potentials. The wavefunction $|\Phi(x,t)\rangle$ of a single atom satisfies the Schrödinger equation,

$$\mathrm{i}\hbar\frac{\partial}{\partial t}|\Phi(x,t)\rangle = (H_M + H_0 + H_1)|\Phi(x,t)\rangle. \tag{3}$$

If we omit the kinetic energy term from the Hamiltonian, we obtain an equation for adiabatic eigenstates, $|\Psi_\alpha(x,t)\rangle$,

$$\mathrm{i}\hbar\frac{\partial}{\partial t}\mathrm{e}^{-\mathrm{i}E_\alpha(x)t/\hbar}|\Psi_\alpha\rangle = (H_0 + H_1)\mathrm{e}^{-\mathrm{i}E_\alpha(x)t/\hbar}|\Psi_\alpha\rangle, \tag{4}$$

where the $|\Psi_\alpha(x,t)\rangle$ are periodic functions and can be expanded as a Fourier series. For a two-level atom, it takes the form

$$|\Psi_\alpha(x,t)\rangle = \sum_{l=-\infty}^{\infty} \exp(-\mathrm{i}l\delta t)[c_g^l(x)|g\rangle + c_e^l(x)|e\rangle]. \tag{5}$$

This results in a Floquet eigenvalue equation for $E_\alpha(x)$, which plays the role of the adiabatic potentials,

$$(V_g(x) - l\delta)c_g^l + \sum_n \frac{\Omega_n}{2} c_e^{l+n-1} = E_\alpha(x)c_g^l, \tag{6}$$

$$(V_e(x) - \delta_1 - l\delta)c_e^l + \sum_n \frac{\Omega_n}{2} c_g^{l-n+1} = E_\alpha(x)c_e^l. \tag{7}$$

The complete wavefunction can then be expanded in a basis of these adiabatic eigenstates, which play the role of Born–Oppenheimer channel functions,

$$|\Phi(x,t)\rangle = \sum_{\alpha} c_{\alpha}(x,t)|\Psi_{\alpha}(x,t)\rangle, \tag{8}$$

resulting in the equation

$$\mathrm{i}\hbar\frac{\partial}{\partial t}c_{\alpha}(x,t) = [H_M + E_{\alpha}(x)]c_{\alpha}(x,t) + \sum_{\beta} H_M^{\alpha\beta}c_{\beta}(x,t), \tag{9}$$

where $H_M^{\alpha\beta} \equiv \langle\Psi_{\alpha}|H_M|\Psi_{\beta}\rangle$. The equations for different α decouple provided that the mixing terms coupling the channels are small. We expect this to be the case provided that the kinetic energy of the atom in the lattice, which is typically on the order of the recoil energy, is much smaller than the separation between the adiabatic potentials, which is characterized by laser parameters, e.g. the Rabi frequency and detuning. Below we will initially neglect these terms, and in section 5, we will discuss in detail non-adiabatic processes, and how they should be suppressed in experimental implementations.

In the case of two-level atoms, the eigenvalues $E_{\alpha}(x)$ of the equations appear in pairs, and may be identified as the upper $V^{+}(x)$ and the lower $V^{-}(x)$ dressed potentials for a given Floquet manifold (see figure 2). The corresponding eigenstates for the adiabatic potentials in general have components from different Floquet manifolds. For the simple case of one dressing field in the off-resonant scheme (with only Ω_1 nonzero), the different manifolds in the Floquet basis decouple, and we only need to diagonalize a two-by-two matrix. In this case, the expression for the adiabatic potential and its corresponding states are:

$$\begin{aligned} V^{\pm} &= -\frac{Z}{2} \pm \sqrt{X^2+Y^2}, \\ |\Psi^{\pm}\rangle &= \frac{1}{2}\left[\left(1 \mp \frac{X}{\sqrt{X^2+Y^2}}\right)^{1/2}|g\rangle \pm \left(1 \pm \frac{X}{\sqrt{X^2+Y^2}}\right)^{1/2}|e\rangle\right], \end{aligned} \tag{10}$$

where $X \equiv V_e(x) - \delta_1/2$ and $Y \equiv \Omega_1/2$, $Z \equiv \delta_1$. The resultant dressed potential has a lattice spacing of $\lambda/4$. The structure of the adiabatic potential becomes more complicated with more dressing fields. With n dressing fields, it is possible to create a lattice with spacing approximately $\lambda/2(n+1)$. This increase in the spatial resolution is at the expense of a decrease in the lattice depth.

2.2. Addressable subwavelength lattices with two-level atoms in 1D: near-resonant scheme

In the near-resonant scheme, the counter-oscillating background potentials are generated by directly coupling the two internal states with standing wave fields, producing a pair of ac-Stark split states. The Hamiltonian describing the coupling between states is now given by (cf equation (2))

$$\begin{aligned} H_0 &= -\delta_0|e\rangle\langle e| + \left(\frac{\Omega_0(x)}{2}|e\rangle\langle g| + \text{h.c.}\right), \\ H_1 &= \sum_{n}\frac{\Omega_n}{2}\exp(-\mathrm{i}n\delta t)|e\rangle\langle g| + \text{h.c.}, \end{aligned} \tag{11}$$

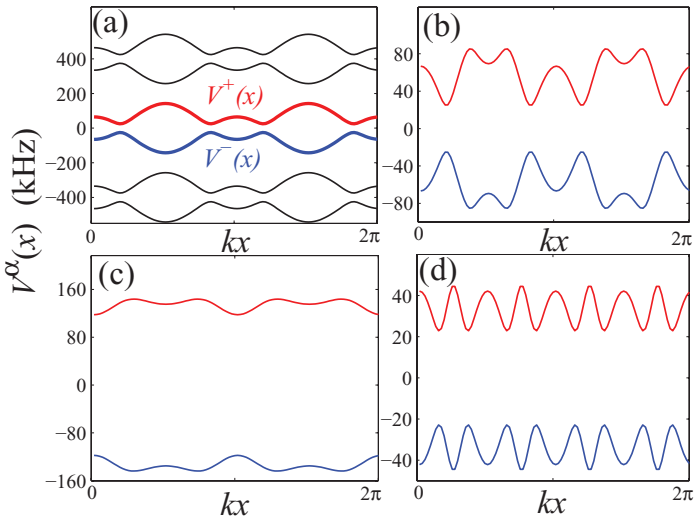

Figure 2. Illustration of the controllability of subwavelength potentials. (a) Typical subwavelength lattice with $n = 1$. The potential in the figure is generated with the off-resonant scheme with the parameters: $V_0 = 200\,\text{kHz}$, $\Omega_1 = 2\pi \times 50\,\text{kHz}$ and $\delta_1 = 120\,\text{kHz}$. Similar potentials can also be generated with the near-resonant scheme. (b) Subwavelength double-well structure generated with the off-resonant scheme with the parameters: $V_0 = 200\,\text{kHz}$, $\Omega_1 = 2\pi \times 50\,\text{kHz}$, $\delta_1 = 120\,\text{kHz}$, $\Omega_2 = 2\pi \times 50\,\text{kHz}$ and $\delta = 220\,\text{kHz}$. The relative depth of the wells in the subwavelength structure can be tuned by changing Ω_2 or δ. (c) Subwavelength double-well structure generated with the near-resonant scheme with the parameters: $\Omega_0 = 2\pi \times 400\,\text{kHz}$, $\delta_0 = 100\,\text{kHz}$, $\Omega_1 = 2\pi \times 560\,\text{kHz}$ and $\delta = -400\,\text{kHz}$. The central barrier height in the lower dressed potential can be adjusted by changing either δ or Ω_1. (d) Subwavelength double-well structure generated with the off-resonant scheme with $n = 3$ dressing fields: $V_0 = 200\,\text{kHz}$, $\delta_1 = 60\,\text{kHz}$, $\Omega_1 = \Omega_2 = \Omega_3 = 2\pi \times 50\,\text{kHz}$ and $\delta = 140\,\text{kHz}$.

where $\Omega_0(x) = \Omega_0 \sin(kx)$ is the Rabi frequency corresponding to a standing wave field, and Ω_n ($n = 1, 2, \ldots$) are the Rabi frequencies of the dressing fields with corresponding detunings $\delta_n = \delta_0 + n\delta$. Note that the background potentials are associated with the eigenstates of H_0, with the values of the potentials and the states given by the same form as equation (10), with $X \equiv -\delta_0/2$, $Y \equiv \Omega_0(x)/2$ and $Z \equiv \delta_0$ [16].

Similar to the procedure in the previous section, we derive the equations for the adiabatic potentials,

$$(-l\delta)c_g^l + \frac{\Omega_0(x)}{2}c_e^l + \sum_n \frac{\Omega_n}{2}c_e^{l+n} = E_\alpha(x)c_g^l, \tag{12}$$

$$(-\delta_0 - l\delta)c_e^l + \frac{\Omega_0(x)}{2}c_g^l + \sum_n \frac{\Omega_n}{2}c_g^{l-n} = E_\alpha(x)c_e^l, \tag{13}$$

with $E_\alpha(x)$ being the adiabatic potentials.

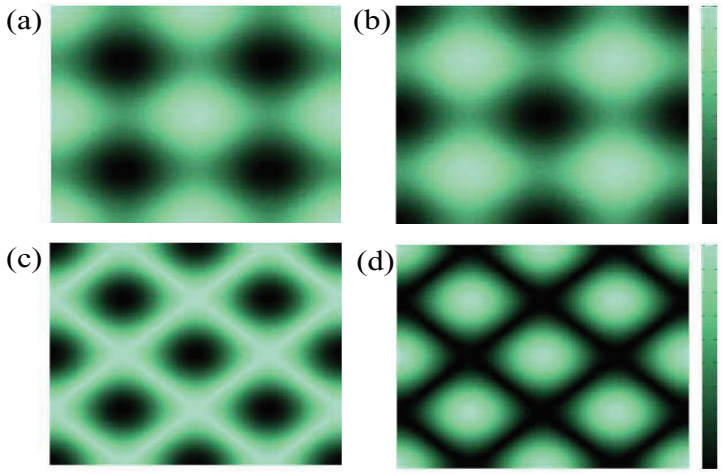

Figure 3. Adiabatic dressed potentials in 2D from an initial square lattice, with depth $2V_0$, formed with a single dressing field, $\delta_1 = 2V_0$. (Note that the potential energy represented by each colour is particular to the figure part, and in each case darker colours correspond to lower potential energy.) (a) The initial off-resonant potential for state $|g\rangle$, $V_g(x, y) = -V_0 \sin^2(k_l x) - V_0 \sin^2(k_l y)$. (b) The initial resonant potential for state $|e\rangle$, $V_e(x, y) = -V_g(x, y)$. (c) The lower dressed potential $V^-(x, y)$, corresponding to a square lattice with $1/\sqrt{2}$ times the original period. (d) The upper dressed potential $V^+(x, y)$, corresponding to interconnected rings. Note that the adiabatic potentials $V^{\pm}(x, y)$ can be found from equation (10), and have a maximum depth V_0, which decreases as the Rabi frequency of the dressing field increases.

In figure 2, we give examples of the flexibility in constructing adiabatic potentials via the near-resonant scheme as well as the off-resonant scheme, including the realization of double-well structures on a subwavelength scale. In figures 2(b) and (c), we demonstrate the simple case of one dressing field: by varying the Rabi frequency or the detuning of the dressing field, the spatial structure and the central barrier height of the subwavelength double-well structure can be controlled. This is essential for entanglement manipulation and state preparation, as we will discuss later.

2.3. Adiabatic potentials in higher dimensions

In higher dimensions, adiabatic potentials can also be used both to create shorter period lattices and to change the geometry of the lattices. Two examples of 2D potentials are shown in figures 3 and 4. In figure 3, we show the form of the dressed potentials obtained with an initial square lattice with period a. From initial off-resonant potentials $V_e(x, y) = V_0 \sin^2(k_l x) + V_0 \sin^2(k_l y)$ and $V_g(x, y) = -V_e(x, y)$, and using a detuning $\delta_1 = 2V_0$, we obtain for $V^-(x, y)$ a square lattice of period $a/\sqrt{2}$, as the minima in this dressed potential occur at each position of a minimum in $V_e(x, y)$ or $V_g(x, y)$. In the upper adiabatic potential $V^+(\mathbf{x})$, we observe the same form inverted, giving rise to a potential consisting of interconnected rings.

In figure 4, we show the dressed potentials arising from an initial triangular lattice, formed by three interfering laser beams at an angle of $\pi/3$ to each other. This produces a well-defined

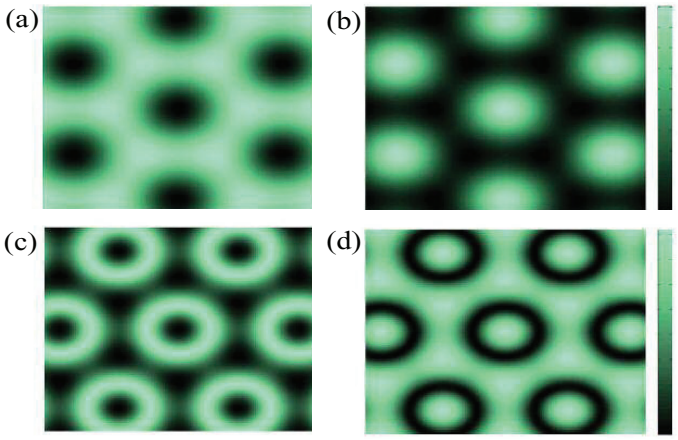

Figure 4. Adiabatic dressed potentials in 2D from an initial triangular lattice, with depth $2V_0$, formed with a single dressing field, $\delta_1 = 2V_0$. (Note that the potential energy represented by each colour is particular to the figure part, and in each case darker colours correspond to lower potential energy.) (a) The initial off-resonant potential for state $|g\rangle$, $V_g(x, y)$. (b) The initial resonant potential for state $|e\rangle$, $V_e(x, y) = -V_g(x, y)$. (c) The lower dressed potential $V^-(x, y)$, corresponding to a honeycomb lattice with additional sites in the centre of a ring-shaped barrier. (d) The upper dressed potential $V^+(x, y)$, corresponding to disconnected rings. Note that the adiabatic potentials $V^{\pm}(x, y)$ can be found from equation (10), and have a maximum depth V_0, which decreases as the Rabi frequency of the dressing field increases.

honeycomb lattice structure, with auxiliary sites introduced in the lower dressed potential, $V^-(x, y)$. In the upper dressed potential, $V^+(x, y)$ we observe a series of disconnected rings (see figure 4(d)). Such disconnected ring structures can also be produced from a square 2D lattice with two dressing frequencies. Note that the control over well depth here could have many useful applications, e.g. in the case of the square lattice it could be well-suited to implementation of ring-exchange Hamiltonians [24].

3. State-dependent subwavelength potentials with multi-level atoms

The ideas for creating addressable, subwavelength lattices for two-level atoms as discussed in the previous section will now be extended to multi-level atoms, where it is possible to create internal state- (qubit-)dependent potentials. We will discuss, in particular, the case of alkaline-earth-like atoms with nonzero nuclear spin, e.g. ^{171}Yb. In addition to the optical excitation to the metastable triplet levels, we have an extra degree of freedom in the form of different magnetic sublevels, which arise from the nuclear spin.

3.1. Off-resonant lattices

3.1.1. Lattice with alkaline-earth-like atoms. As an example, we consider the level structure of ^{171}Yb, for which the nuclear spin $I = 1/2$. We will make use of the states on the clock transition. The states in the ground state manifold are $|^1S_0, m_I = \pm 1/2\rangle$, and those in the

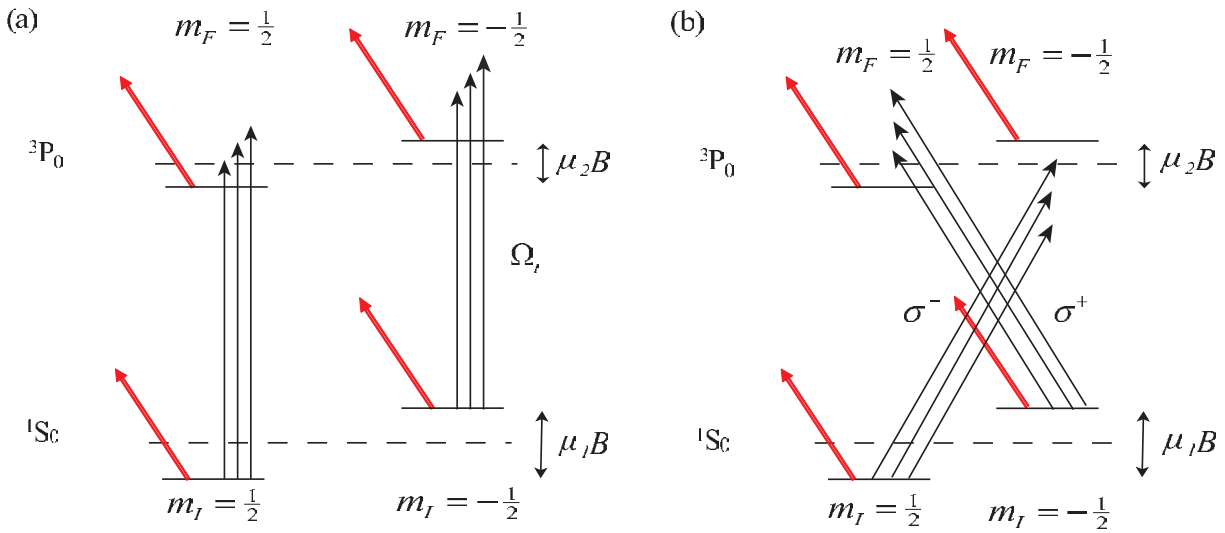

Figure 5. Atomic level structure and laser configurations for the generation of sub-wavelength lattices in ^{171}Yb from off-resonant background potentials, which are formed by ac-Stark shifts represented by the red arrows. (a) Formation of subwavelength lattices in two two-level systems with π-polarized dressing fields (black arrows), where the magnetic field induces differential Zeeman shifts in the $^1S_0$ ($\mu_1 \sim 760\,\mathrm{Hz\,G^{-1}}$), and the $^3P_0$ ($\mu_2 \sim 350\,\mathrm{Hz\,G^{-1}}$) manifolds [28]. (b) Formation of subwavelength lattices in two two-level systems with circularly polarized dressing fields (black arrows).

excited state manifold are $|^3P_0, m_F = \pm 1/2\rangle$. It is also possible to generalize the scheme to other alkaline-earth-like atoms with nonzero nuclear spin, e.g. ^{87}Sr ($I = 9/2$), though one then needs to carefully choose the working states in the hyperfine structure [25, 26].

To generate off-resonant subwavelength lattices, we induce opposite background potentials for the states on the clock transition. This is done by applying a set of standing wave laser fields at a specific 'anti-magic' wavelength at which the ac polarizability of the manifolds $^1S_0$ and $^3P_0$ are exactly opposite. This is exactly the opposite case to that used in optical lattice clock experiments [19, 20, 27], where a 'magic' wavelength is chosen so that the ac-Stark shifts of the clock states are equal. (We expect that the 'anti-magic' wavelength in our case to be ~ 600 nm for ^{171}Yb, and the resultant ac-Stark shift on the order of several hundred kHz for a laser intensity of $I \sim 10\,\mathrm{kW\,cm^{-2}}$.) Once the background potentials are generated, we can couple these potentials by applying additional optical dressing fields tuned near the resonance of the clock transition $^1S_0$– $^3P_0$ at ~578 nm. Atoms can be loaded into the minima of the upper (lower) adiabatic potential by first preparing them in one of the manifolds $^1S_0$ or $^3P_0$, and then appropriately ramping up the dressing fields adiabatically.

As shown in figure 5(a), the $^1S_0$ and $^3P_0$ manifolds for ^{171}Yb are each split into two sublevels. This gives us a four-level system, and dressing fields coupling the different manifolds can be produced using either π-polarized or circularly polarized light. In the appendix, we summarize the origins of the corresponding matrix elements [29, 30]. Note, in particular, that the matrix elements for circularly polarized couplings are nonzero as a result of contributions in the $^3P_0$ manifold from other levels due to hyperfine mixing [29, 30]. In the case where

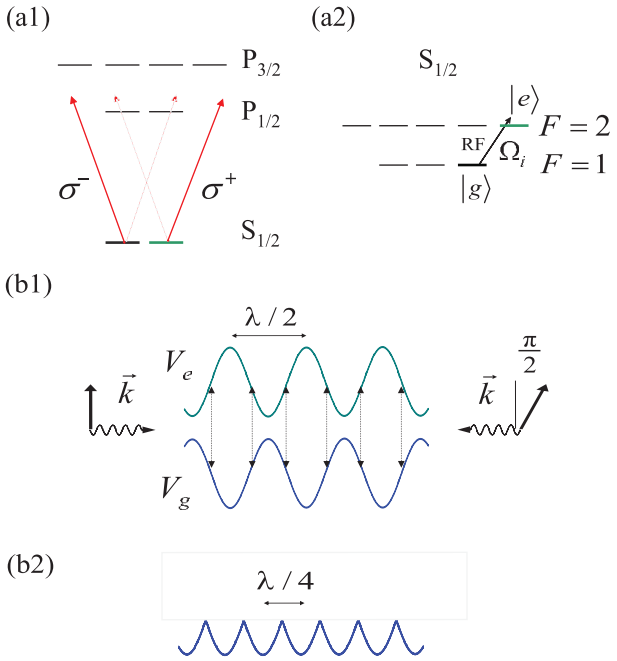

Figure 6. Schematics for the generation of an off-resonant subwavelength lattice with ^{87}Rb. (a1) Lights of different circular polarization are tuned near the centre of the fine structure splitting to generate spin-dependent potentials. (a2) and (b1) RF fields are applied to couple different hyperfine states with counter-oscillating potentials, which are generated by shifting the spin-dependent potentials. (b2) The resultant adiabatic potential in the case of one dressing field has a lattice spacing $\lambda/2$, with λ the wavelength of the laser generating the spin-dependent potentials in (a1).

we use only circularly polarized dressing fields, we will produce two independent two-level systems, where the resulting subwavelength lattice can be manipulated for each by altering the appropriate component of each circular polarization in the dressing field. For π-polarized light, we also obtain two independent two-level systems, in which we can offset the relative well depths by applying an external magnetic field. Due to the differential Zeeman shift in the $^1S_0$ and $^3P_0$ manifolds [28], this will alter the detunings of the dressing fields, as well as the energies of the uncoupled internal states. For example, with the laser parameters: $V_0 = 200\,\text{kHz}$, $\Omega_1 = 2\pi \times 200\,\text{kHz}$, $\delta_1 = 200\,\text{kHz}$, and under a small magnetic field of $B = 10\,\text{G}$, the estimated energy difference between the potentials corresponding to the two different dressed states at $kx = \pi/2$ is $\sim 7\,\text{kHz}$, and at $kx = \pi$ is $\sim 4\,\text{kHz}$. These numbers increase significantly as the external magnetic field is increased. This allows the state to be rotated between dressed states of the different two-level systems selectively for different wells of the substructure using RF coupling fields. This would be useful for applications to quantum information processing (see below).

3.1.2. Lattice with alkali atoms. One may also generate off-resonant subwavelength lattices with alkali atoms. Here, the counter-oscillating background potentials should be produced for two different hyperfine ground states making use of well known ideas to produce spin-dependent lattice potentials [31, 32], as shown in figure 6. These spin-dependent lattice potentials can

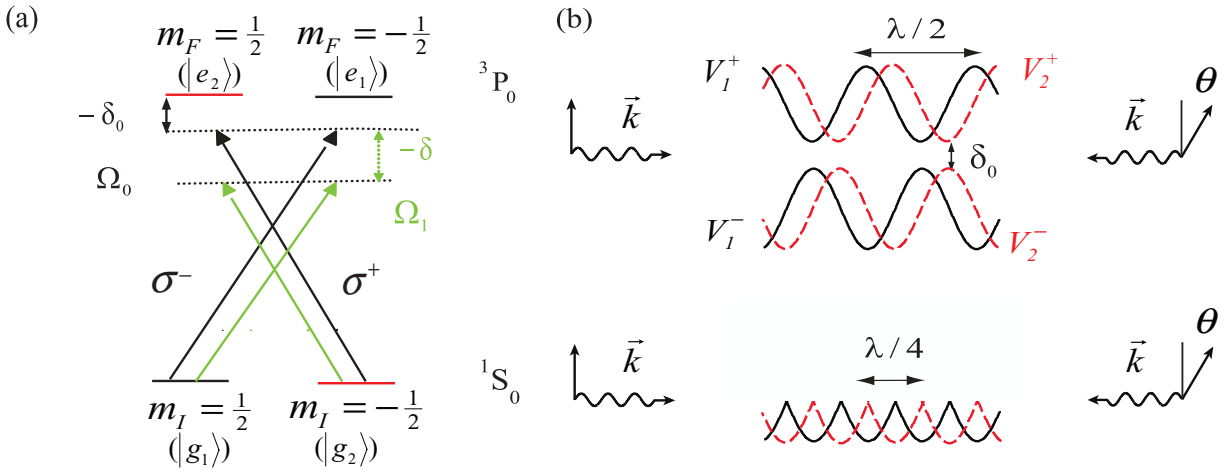

Figure 7. (a) Level structure and laser configurations for the generation of near-resonant subwavelength potentials with ^{171}Yb using cross-coupling dressing fields. (b) Upper panel: with only the coupling laser Ω_0, there are two independent sets of spin-dependent lattice potentials $V_i^{\pm}(i = 1$ and $2)$, where i labels the two different sets of potentials created by lasers with different polarization and $\pm$ labels the upper/lower potential in a given set. The relative position of the two sets of potentials can be adjusted by varying θ in the lin-$\angle$-lin configuration. The lattice spacing in this case is still $\lambda/2$. Lower panel: by adding one dressing field Ω_1, the lower potential, become state-dependent subwavelength potentials, with lattice spacing $\lambda/4$. The relative positions of the two lower potentials can be adjusted by varying θ.

then be coupled using RF dressing fields to produce subwavelength optical lattices. Details of this scheme are summarized in the caption of figure 6. Note that with alkali atoms it is not straightforward to find combinations of states that act as independently coupled two-level systems and that are simultaneously collisionally stable. This will limit the application of alkali atoms in generating state-dependent subwavelength potentials, as well as in entanglement operations, as we will discuss later for alkaline-earth-like atoms. In addition, with alkali atoms, the two hyperfine ground states used to generate the dressed potentials decohere quickly in the presence of magnetic field fluctuations, which is not the case with alkaline-earth-like atoms, where the dressed potentials are generated almost purely from nuclear spins.

3.2. Near-resonant lattices

3.2.1. Lattice with alkaline-earth-like atoms. The long-lived $^3P_0$ level motivates the application of near-resonant lattices, as discussed previously in section 2.2, with direct coupling with a standing wave field tuned to the clock transition producing counter-oscillating dressed potentials. The great advantage here, though, is that we can now produce these background potentials with lights of two different circular polarizations, generating two sets of independent background potentials (see figure 7(a)). We can take advantage of this in two ways: (i) we can couple these potentials with circularly polarized dressing fields (see figure 7), so that we produce two independent sets of addressable subwavelength lattices; or (ii) we can couple

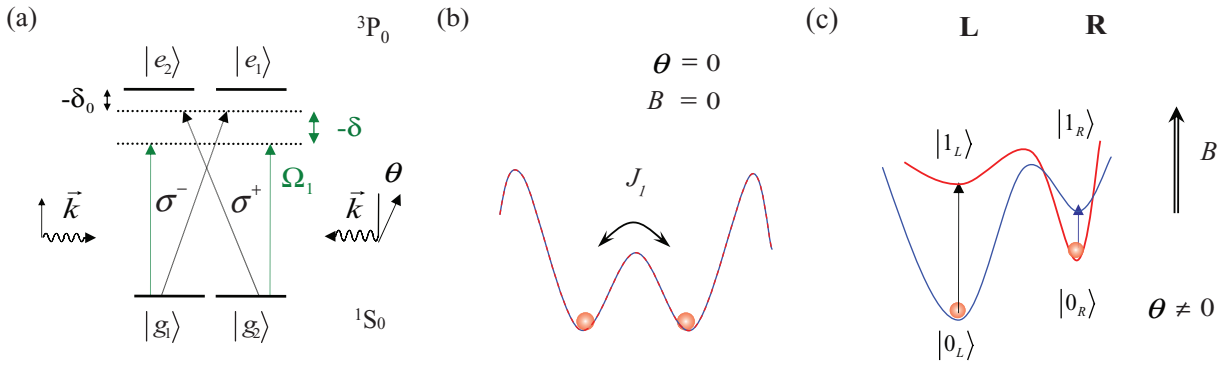

Figure 8. (a) Level structure and laser configurations for the generation of near-resonant subwavelength potentials with ^{171}Yb using π-polarized dressing fields. (b) Atoms in the subwavelength double-well structure can be entangled by a controlled evolution with the exchange interaction turned on. The interaction can be switched on and off by varying the height of the central barrier. (c) In the presence of a small magnetic field and as the angle in the lin-$\angle$-lin configuration $\theta \neq 0$, atoms with different internal states in the double-well structure, which can be defined as qubit states $|0_i\rangle$ and $|1_i\rangle$ (where $i = \mathrm{L}$ and R) as in the figure, feel different potentials. Atoms within the subwavelength structure can thus be selectively addressed.

these potentials with π-polarized fields, so that we form dressed states with all four levels (see figure 8(a)), and use this to engineer particular forms for the potentials. For the convenience of discussion, we define the notation for the internal states $|g_1\rangle = |^1\mathrm{S}_0, m_\mathrm{I} = +1/2\rangle$, $|g_2\rangle = |^1\mathrm{S}_0, m_\mathrm{I} = -1/2\rangle$, $|e_1\rangle = |^3\mathrm{P}_0, m_\mathrm{F} = -1/2\rangle$ and $|e_2\rangle = |^3\mathrm{P}_0, m_\mathrm{F} = +1/2\rangle$.

In the first case, where the states are cross-coupled as shown in figure 7, we then produce state-dependent lattices in the sense that we have two independent two-level systems, in which we form dressed states of $|g_i\rangle$ and $|e_i\rangle$ ($i = 1$ and 2) for each i independently. Both the near-resonant background potentials and the final subwavelength potentials are internal-state dependent, and can be easily manipulated independently. For example, using lasers in a lin-$\angle$-lin configuration (two counter-propagating, linearly polarized beams with a relative polarization angle θ), the lattices can be relatively shifted by varying θ [31, 32] (see figure 7(b)). Such spin dependence could be used similarly to the case in alkali atoms [31, 32], and we expect losses due to spontaneous emissions to be strongly suppressed in the present case. Note that the dipole matrix element for the cross coupling is given by $2\pi\epsilon_0\hbar c^3\Gamma/(\omega_0^3)$, where ω_0 is the frequency of the clock transition $^1\mathrm{S}_0$– $^3\mathrm{P}_0$, and $\Gamma \sim 2\pi \times 10$ mHz is the natural linewidth of the $^3\mathrm{P}_0$ state in ^{171}Yb [27]–[30] (see appendix for more details).

Subwavelength addressability can be achieved in this configuration in a manner similar to that discussed in the previous section. By preparing the atoms near the minima of the lower adiabatic potentials and applying an external magnetic field to lift the degeneracy of the states in the subwavelength structure, we can perform rotations between the independent two-level systems selectively well within the subwavelength structure.

In the second case, we consider using π-polarized dressing fields as shown in figure 8. Here, all the states are coupled to make the adiabatic potentials, and changing the angle θ in the lin-$\angle$-lin configuration modifies the shape of all the four adiabatic potentials in each Floquet

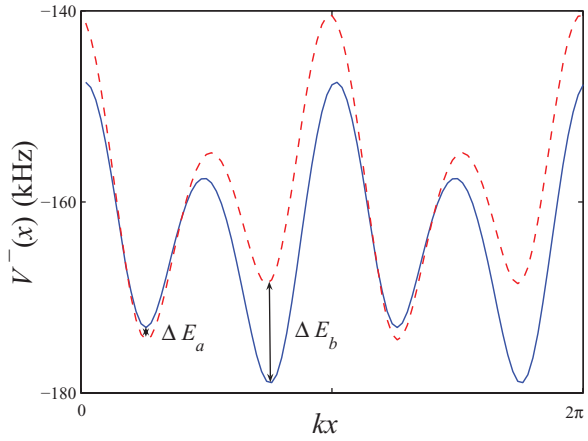

Figure 9. Biased double-well structure generated with the configuration in figure 8 for subwavelength addressing with ^{171}Yb. The two originally degenerate potentials (the dashed and the solid curve) are shifted relative to each other under a small bias magnetic field, and with a finite angle θ in the lin-$\angle$-lin configuration as shown in figure 8(a). Parameters: $\Omega_0 \sim 2\pi \times 400\,\text{kHz}$, $\delta_0 \sim -100\,\text{kHz}$, $\delta \sim -420\,\text{kHz}$, $\Omega_1 = 2\pi \times 480\,\text{kHz}$, $\theta = 0.1$ and $B = 10\,\text{G}$. The energy shifts are $\Delta E_a \sim 1.3\,\text{kHz}$ and $\Delta E_b \sim 11\,\text{kHz}$, respectively.

manifold. In this configuration, it is possible to produce a repeated double-well potential, in which the two wells can be individually addressed. This is done by first setting the angle θ in the lin-$\angle$-lin configuration to a small but nonzero value. This will change the shape of the potentials and lift the symmetry in the double-well structure. An example is given in figure 9, where at $\Omega_0 \sim 2\pi \times 400\,\text{kHz}$, $\Omega_1 \sim 2\pi \times 480\,\text{kHz}$, $\delta_0 \sim -100\,\text{kHz}$, $\delta \sim -420\,\text{kHz}$, $\theta = 0.1$ and $B = 10\,\text{G}$, the energy shifts are $\sim$1.3 and $\sim$11 kHz for the two sub-wells, respectively. Atoms in the left and right hand side of the double-well structure can then be rotated selectively by a RF coupling after the application of an external magnetic field to shift the potentials.

In practice, strong coupling at intensity I on the clock transition will also give rise to ac-Stark shifts ΔE of the states $|e_i\rangle$ and $|g_i\rangle$, which, as $\Delta E \propto I$ and $\Omega \propto \sqrt{I}$, will become important at large fields (e.g. $\sim 10\,\text{kW cm}^{-2}$ for ^{171}Yb [33]). These have been neglected in the two-level atom picture presented in section 2.2. At higher fields, we essentially obtain a combination of the off-resonant and near-resonant background potentials. If the polarizability of $^3\text{P}_0$ and $^1\text{S}_0$ are opposite, it will simply enhance the depth of the resulting potentials. These combined adiabatic potentials are still spin-dependent as the ac-Stark shifts lose their spatial dependence as the angle θ is increased to $\theta = \pi/2$. In the case that these polarizabilities have the same sign, the ac-Stark shift can also be cancelled or modified by an additional laser at a different wavelength.

3.2.2. Lattice with alkali atoms. With alkali atoms one could also form near-resonant lattices by coupling different hyperfine ground states in the $S_{1/2}$ level, e.g. via a Raman process. If the Raman process beams have a sinusoidally varying effective Rabi frequency, this will then generate two counter-oscillating dressed states. These can be coupled by RF dressing fields to form subwavelength lattice potentials. However, this does not give rise to simple internal state-dependent lattices as in the case with alkaline-earth-like atoms.

4. Application of subwavelength lattices in quantum simulation and quantum information

Having established the methods to realize subwavelength lattice potentials, we now turn to discuss ways to utilize the flexibility in control of the potentials for applications in quantum simulation and quantum information. This requires consideration of the many-body physics in these potentials. We will show how a generalized Hubbard model can be realized by engineering the subwavelength potential. This generalized single-band Hubbard model features fast tunnelling rates due to the small spatial separation of different wells in the potential, which can be utilized to improve the timescales associated with realization of interesting quantum phases and entanglement via exchange interactions.

4.1. Single-band Hubbard model for the subwavelength lattice

We begin by considering the simplest case of the off-resonant scheme with a sinusoidal lattice in 1D, beginning with two background counter-oscillating potentials $V_e(x) = -V_g(x) = V_0 \sin^2(kx)$, as discussed in section 2.1. We then choose the detuning and Rabi frequency of n dressing transitions so that the resulting bound states in each well of the adiabatic potential have approximately the same energy. In this way a subwavelength lattice will be formed in which the lattice spacing scales approximately as $\lambda/[2(n+1)]$, while the depth V_n of the potential can be as large as $V_n \sim V_0/(n+1)$ and decreases with increasing Rabi frequency Ω_n. Motion can be considered in the tight-binding limit of the resulting lattice model provided $V_n/[(n+1)^2] \gtrsim 5E_{\mathrm{R}}$, and the dynamics are described by the single-band Hubbard model

$$\hat{H} = -\sum_{\langle\alpha,\beta\rangle} J_{\alpha\beta} c_\alpha^\dagger c_\beta + \sum_\alpha \Delta_\alpha c_\alpha^\dagger c_\alpha + \sum_{\alpha,\beta} U_{\alpha\beta} c_\alpha^\dagger c_\beta^\dagger c_\beta c_\alpha. \tag{14}$$

Here, c_α is the annihilation operator for the bosonic or fermionic atoms, with α specifying the lattice site and internal atomic (spin) state, $J_{\alpha\beta}$ denotes the tunnelling rates. We denote by Δ_α the energy offset for the internal state and lattice site specified by α, and $U_{\alpha\beta}$ are the collisional interaction energies, which follow from our knowledge of the potentials and scattering properties. A single-band Hubbard model is valid provided all of these energies are smaller than the separation energy to higher bands, which, in the case that the lowest bound states in all wells have the same energy, is bounded above by the oscillation frequency in a typical well, $\omega = [4d_1 V_0 E_{\mathrm{R}}/(d_1^2 + \Omega_1^2)^{1/2}]^{1/2}/h$.

If we choose the detunings of the n dressing transitions so that Δ_α is constant, then in 1D, $J_{\alpha\beta} = J_n \delta_{\alpha+1,\beta}$ can be estimated via a simple rescaling of the recoil energy $E_{\mathrm{R}} = \hbar^2 k^2/2m$, as

$$\frac{J_n}{E_{\mathrm{R}}} \sim 4\left(\frac{n+1}{\pi}\right)^{1/2}\left(\frac{V_n}{E_R}\right)^{3/4} \exp\left(-\frac{2}{n+1}\sqrt{\frac{V_n}{E_{\mathrm{R}}}}\right). \tag{15}$$

Here, the tunnelling rates increase exponentially with increasing n. Note, however, that these rates can vary within the substructure, because the wells with $n > 1$ dressing frequencies will not be exactly symmetric, and this can give rise to small splittings within the lowest Bloch band. In figure 10, we plot values of J_n for varying depths of the background potential, and number of dressing transitions n. We will typically have onsite interactions only, which can be controlled via the shape of each well and the scattering lengths for atoms in the different internal states $|e\rangle$ and $|g\rangle$. This can give rise to generalized Hubbard models, where the onsite interaction changes values between neighbouring sites. Such models can support non-trivial phases, such

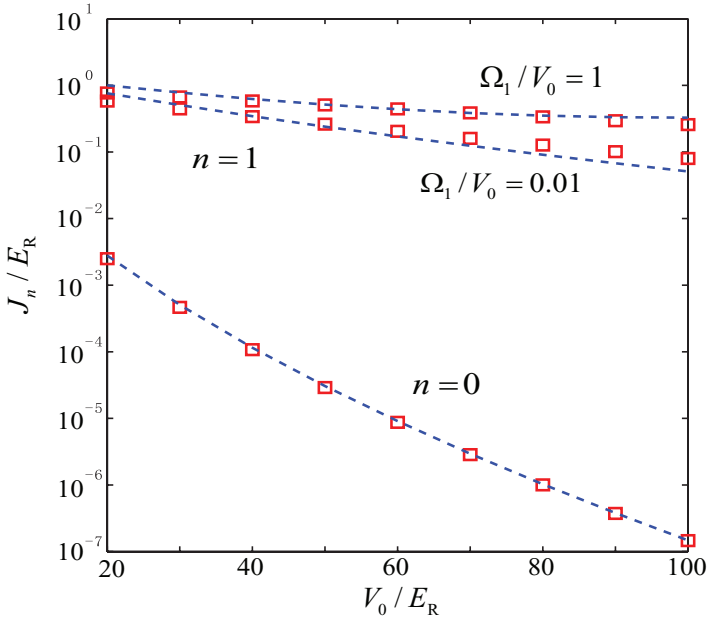

Figure 10. Tunnelling rate J_n in the presence of n dressing fields as a function of V_0/E_R. The squares are numerically obtained values for the case $n = 0$ (lowest curve) and $n = 1$ (upper two curves), respectively. The dotted lines are plots of the n-dependent scaling function (see equation (15) in the text). The lowest curve is for the case $n = 0$ and the higher two curves are for the $n = 1$ case.

as coexisting Mott insulating and superfluid phases [34]. Note that when there is only one dressing frequency $n = 1$, the value of $U_{\alpha\beta}$ is approximately the same as the corresponding onsite interaction in the original background lattice potentials, as the curvature of the wells is essentially unchanged.

4.2. Applications to quantum information

As discussed in section 3.2, we have with ^{171}Yb the possibility to form different addressable subwavelength lattices from four internal states. We have different possibilities then to encode qubits and generate entanglement depending on our choice of configurations for the dressing transitions.

In the case that we choose circularly polarized dressing transitions (see figure 7), we obtain two independent two-level systems, for which we can control the subwavelength lattices independently (see section 3.2). We can then encode qubits on the dressed states of the two two-level systems. These can be addressed individually within the substructure of the subwavelength lattice (i.e. modulo the period of the background potentials, where other recent ideas could be applied to provide addressing on the larger length scale [35]). We can then make use of the state-dependent lattice potentials to perform entangling operations, e.g. using controlled collisions [31, 32].

Another possibility arises in the case that we use π-polarized dressing fields and form adiabatic eigenstates combining all four internal states (see section 3.2 and figure 8). Here, it is possible to create entanglement for fermionic atoms such as ^{171}Yb within the

double-well structure using exchange interactions [3, 36], where the fast tunnelling rates $J_{\alpha\beta}$ between neighbouring wells give rise to faster gate times than are possible without subwavelength lattices. This leads to quantum gate schemes in the spirit of the Loss–DiVincenzo proposal for quantum dots [37], which is based on encoding qubits on electron spins in electrically gated quantum dots, and performing entangling operations using exchange interactions between neighbouring dots by ramping down the corresponding potentials. The same techniques can be applied here. We consider the two-dressed states of our four initial internal levels that have the same dressed potentials, and define these to be our qubit states. We then consider the dynamics generated by the Hamiltonian in equation (14), but now with the tunnelling parameters $J_{\alpha\beta}$ determined by our choice of subwavelength lattices with repeated double-well potentials. The tunnelling between these wells can be made negligible on the timescale of the experiment, so that the dynamics within each double-well is independent. We then have a situation very similar to that discussed in the analysis of spin-exchange gates, e.g. in [3], leading from the two-site double-well potential to exchange interactions between the spin states in each well, given by $H_{\mathrm{SE}} = J_1 \vec{\sigma}_{\mathrm{L}} \cdot \vec{\sigma}_{\mathrm{R}}$, where $J_1 \equiv J^2(1/U_{\mathrm{L}} + 1/U_{\mathrm{R}})$. Here, σ_{L} and σ_{R} represent the spin operators in the left and right well, respectively, where the spin in each well corresponds to a two-state system consisting of the two different dressed states we are considering. The coefficient J_1 is determined from the tunnelling amplitude between sites, $J = J_{\alpha\beta}$ (see equation (14)); and the onsite interaction strengths U_{L} and U_{R}, between two atoms, one in each state, in the left well and right well, respectively.

In the context of electrically gated quantum dots, one of the most challenging aspects of implementing quantum computing is to achieve local addressing of the qubits. As described above, this is made possible here by the addressability of the individual wells within the subwavelength structure, as discussed in section 3.2. There we specifically discussed rotation between different qubit states. However, it is also possible to perform readout state-selectively by creating an energy offset between the two qubit states by introducing an external magnetic field, and then coupling them state-selectively to the $^3\mathrm{P}_2$ level. This is possible because the $^3\mathrm{P}_2$ level has a very small natural linewidth $\Gamma \sim 2\pi \times 15\,\mathrm{mHz}$ [29], so that coupling to this level can be easily made frequency-selective. Coupling between the qubit states and $^3\mathrm{P}_2$ can be generated with a Raman pulse, making use of the larger coupling elements of both $^3\mathrm{P}_2$ and $^3\mathrm{P}_0$ to high-lying states such as $^3\mathrm{S}_1$.

5. Landau–Zener-type losses

As discussed in section 2.1, one of the major limitations of the adiabatic potentials is the loss of atoms via the Landau–Zener-type processes. These losses correspond to the tunnelling of atoms from a given adiabatic potential into the continua of other adiabatic potentials. In the following, we show that these processes can be made exponentially small by increasing the laser power.

The Landau–Zener-type losses can be understood by looking at the simple scenario of a single avoided crossing of two adiabatic potentials. This problem has been discussed in detail in [16], where the two adiabatic potentials $\pm U(x)$ are generated by coupling a two-level atomic system using a standing wave light field with spatially oscillating Rabi-frequency. The loss rate Γ of a particle from the bottom of a well of the upper adiabatic potential $U(x)$ into the continuum spectrum of $-U(x)$ can be estimated semiclassically for a small violation of

adiabaticity:

$$\Gamma \sim \Gamma_0 \exp\left[2\mathrm{i}\int_0^{x_0}(p_+ - p_-)\right], \tag{16}$$

where $p_\pm = \sqrt{2m[E \mp U(x)]}$, E is the energy of the atom and x_0 is determined by the saddle-point condition $p_+(x_0) = p_-(x_0)$. The quantity Γ_0 is the attempt frequency, which is of the order of the oscillation frequency ω of a particle at the bottom of the upper potential $U(x)$ [38, 39]. This analysis, in particular equation (16), can be directly adopted for the estimation of the Landau–Zener-type loss rate from the upper adiabatic potential in the simple case of one dressing field in the off-resonant scheme and no dressing field in the near-resonant scheme.

For the off-resonant scheme with only one dressing field, and for a detuning $\delta_1 = V_0$, the adiabatic potentials can be written as $\pm U(x)$, where $U(x) = \sqrt{V(x)^2 + \Omega_1^2/4}$ and $V(x) = V_0 \sin(2kx)/2$. In the vicinity of the saddle point $x_0 = 0$, the background potential can be linearized $V(x) \sim V_0 kx$, and we take the energy of the atom $E = U(x_0)$. We may then Taylor expand the adiabatic potentials near the saddle point, $U(x) \sim \Omega_1/2 + m\omega^2 x^2/2$, where $\omega \equiv 2\sqrt{V_0^2 E_\mathrm{R}/\Omega_1}$ with $E_\mathrm{R} = \hbar^2 k^2/2m$ being the recoil energy in the original normal lattice. With these one may carry out the integral in equation (16) explicitly and we get for the loss rate:

$$\Gamma \sim \Gamma_0 \exp\left[-\alpha\frac{\Omega_1}{\omega}\right] = \Gamma_0 \exp\left[-\alpha\frac{\Omega_1^{3/2}}{2V_0 E_\mathrm{R}^{1/2}}\right], \tag{17}$$

where the dimensionless parameter $\alpha \simeq 1.32$ in this case. Note that Ω_1 characterizes in this case the energy separation between the adiabatic potentials. Equation (17) is different from the scaling relation of a typical Landau–Zener transition, where the exponent in the loss rate scales with the energy separation squared. One may recover this typical scaling relation by examining the loss rate of atoms with higher energies in the adiabatic potential.

For the near-resonant lattices, different manifolds in the Floquet basis only decouple in the absence of dressing fields. In this case, we have only the background potentials $\pm U(x)$ resulting from the ac-Stark splitting, where $U(x) = \sqrt{\delta_0^2/4 + \Omega_0(x)^2/4}$. We may also integrate equation (16) to calculate the loss rate from the upper background potential:

$$\Gamma \sim \Gamma_0 \exp\left[-\alpha\frac{\delta_0}{\omega'}\right] = \Gamma_0 \exp\left[-\alpha\frac{\delta_0^{3/2}}{\Omega_0 E_\mathrm{R}^{1/2}}\right], \tag{18}$$

where $\omega' \equiv \sqrt{\Omega_0^2 E_\mathrm{R}/\delta_0}$, with $\alpha \simeq 1.32$. In this case, δ_0 characterizes the energy separation between the background potentials.

These results suggest that the loss rate from the upper adiabatic potential can be made exponentially small by increasing the ratio of the energy difference of the two potentials and the frequency of the atomic motion in the trap. In the simple cases above, this translates to large the Rabi frequency $\Omega_1 \gg E_\mathrm{R}$ in the off-resonant case, and large detuning $\delta_0 \gg E_\mathrm{R}$ in the near-resonant case.

When more complicated lattice potentials are considered, the loss rate due to this Landau–Zener-type transition should in general be computed numerically. However, simple estimates of the loss rates can be obtained by assuming that for a given adiabatic potential the loss is dominated by the leak into the continua of the adiabatic potentials which are closest in energy. If we assume that the loss into the continuum of each potential is independent, the matrix

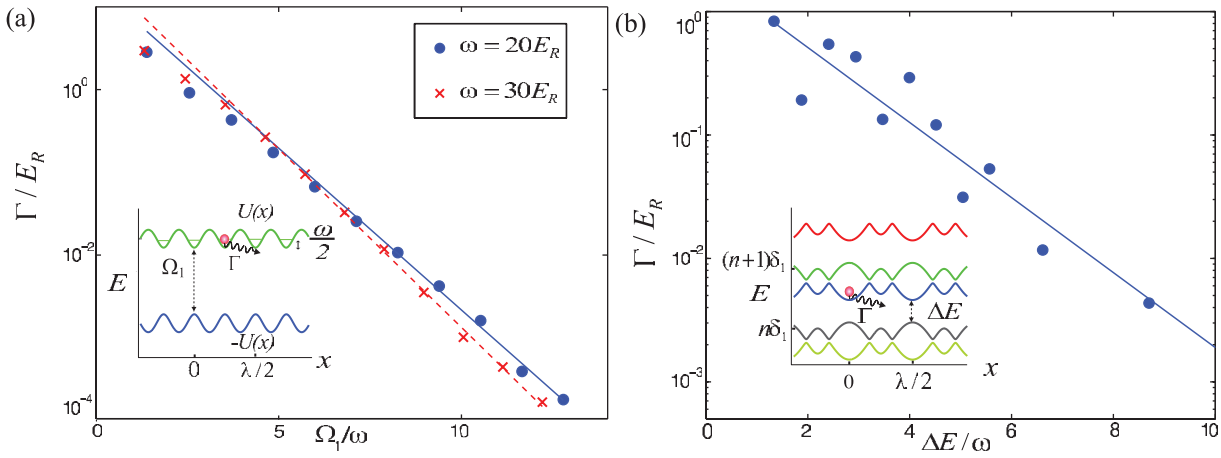

Figure 11. Landau–Zener losses from a $\lambda/4$ lattice, formed with one dressing transition: (a) numerical simulation results for loss rates for atoms in the bound state of the higher energy adiabatic potential in the off-resonant scheme. The solid line is an exponential fit to the result. (inset) The corresponding adiabatic potentials with parameters: $V_0 = 35E_{\mathrm{R}}$, $\Omega_1 = 30E_{\mathrm{R}}$ and $\delta_1 + \delta = 35E_{\mathrm{R}}$. (b) Numerical calculations of the decay rate for atoms in the narrower wells in the low energy adiabatic potential in the near-resonant scheme. (inset) Typical potentials in the limit where the Floquet manifolds are weakly coupled ($\Omega_1 \ll \Omega_0$), with a series of Floquet manifolds each containing two dressed potentials. Parameters: $\Omega_0 = 31E_{\mathrm{R}}$, $\delta_0 = -15E_{\mathrm{R}}$, $\Omega_1 = 2E_{\mathrm{R}}$ and $\delta_1 = -\delta_0 + \left(\sqrt{\delta_0^2 + \Omega_0^2} + \delta_0\right) \times 0.8$.

elements for the decay into the continuum of any one of these nearest adiabatic potentials will have the form equation (16) under the semiclassical approximation. An exponential dependence of the decay rate Γ on the energy separation between the adiabatic potentials is then obtained, similar to equations (17) and (18). Numerically, we find the dimensionless parameter α to be on the order of unity or larger when the laser parameters, e.g. Rabi frequencies and detunings, are much larger than the recoil energy E_{R}. This implies that the loss rate Γ can always be made exponentially small by increasing the laser power.

To check the general conclusion drawn above, we have also performed numerical simulations of the real time evolution of the atoms trapped in the adiabatic potentials by integrating the Schrödinger equation for the full Hamiltonian in the Floquet basis. The atom is initially prepared in the ground state of a potential well, and transition rates are extracted from the projection of the wavefunction onto the manifold corresponding to the initial adiabatic potential as a function of time. For the simple case in figure 11(a), we vary Ω_1 for fixed trapping frequency in the wells of the adiabatic potential $\omega = 2\sqrt{V_0^2 E_{\mathrm{R}}/\Omega_1}$. For a large gap between the potentials, the loss rate scales exponentially as $\Gamma/E_{\mathrm{R}} \propto \exp(-\alpha\Omega_1/\omega)$, as shown by the exponential fit (solid line), which is in agreement with the semiclassical calculation. From the fit, the factor α is estimated to be $\alpha \sim 0.9$ and 1.2 for the exact and linearized potentials, respectively, slightly smaller than the results in the semiclassical approximation.

In the case of near-resonant scheme, as in figure 11(b), we fix $\sqrt{\Omega_0^2 E_R/|\delta_0|} = 30E_R$, and vary the energy gap ΔE between the adiabatic potentials. We again observe an exponential scaling, $\Gamma \propto \exp(-\alpha' \Delta E/\omega)$ (solid line), where the trapping frequency $\omega \approx 15E_R$. In conclusion, we see one can always avoid large Landau–Zener-type losses from the adiabatic potential by increasing the laser power to make the background potential sufficiently deep.

6. Summary and conclusion

To summarize, we have discussed various schemes for the generation of subwavelength lattices with either alkali or alkaline-earth-like atoms. The lattice spacing in these adiabatic potentials can be much smaller than the wavelength of the laser that creates the lattice potential, depending on the number of the additional dressing lasers. The enhanced tunnelling rate one gets from the reduced lattice spacing may be useful for the engineering of generalized Hubbard models for quantum simulation, or for the design of fast quantum gates for quantum computation. The adiabatic potentials in dimensions higher than 1D may also have interesting structures, i.e. disconnected ring potentials in 2D, which is useful for the realization of interesting phases. The first experimental steps in this direction have been recently been reported in [40]. While we have discussed addressable lattices within a $\lambda/2$ period, addressing on a larger scale can be introduced using magnetic or electric field gradients, or other recently proposed techniques [35], [41]–[43]. This, combined with the gate operation, holds the prospect for the realization of general quantum computation in this system. We have also discussed in detail the Landau–Zener-type losses from the adiabatic potentials. We have shown that the loss rate can always be made small at the expense of laser power. For a large number of dressing fields, i.e. for small lattice spacing, the Landau–Zener-type loss would become considerable, and would be the practical limitation on how small a lattice spacing one can get in generating the subwavelength lattices.

Acknowledgments

We thank H P Büchler, A V Gorshkov, S Kotochigova, I Lesanovsky, M D Lukin, A Micheli, V Pal'chikov, T Porto, Y Takahashi, J Ye and T Zelevinsky for interesting discussions. This work was supported by the Austrian FWF through project SFB F15 and by the EU networks OLAQUI and SCALA.

Appendix. Alkaline-earth-like atoms and the clock transition

In this appendix, we examine in detail the matrix element for the clock transition $^1S_0$– $^3P_0$ in alkaline-earth-like atoms. For a detailed discussion, please refer to [29, 30].

We consider the matrix element $\langle {}^1S_0, Im_I|D|{}^3P_0, Fm_F\rangle$, where D is the electric-dipole operator. In the presence of a hyperfine interaction, $|{}^3P_0, Fm_F\rangle$ is not an eigenstate of the system. Under the first order perturbation, the correction to the hyperfine sublevels in $^3P_0$ manifold can be written as:

$$\sum_{\gamma} |\gamma, J, Fm_F\rangle \frac{\langle \gamma, J, Fm_F|V_{hf}|{}^3P_0, Fm_F\rangle}{E(\gamma) - E({}^3P_0)}, \tag{A.1}$$

where γ labels the manifolds that the state is coupled to, and $V_{\rm hf}$ is the hyperfine interaction. Due to the scalar nature of $V_{\rm hf}$, the total angular momentum F and its projection on the z-axis $m_{\rm F}$ are good quantum numbers, as is shown in the expression above. As we are only interested in the E1 transitions from $^1{\rm S}_0$ to $^3{\rm P}_0$, we only consider the nuclear magnetic dipole contribution in the hyperfine interaction, which fixes $J = 1$ in the expression above.

The matrix element for the clock states then becomes:

$$\langle {}^1{\rm S}_0, I m_{\rm I}|D|{}^3{\rm P}_0, F m_{\rm F}\rangle$$
$$= \sum_{\gamma} \langle {}^1{\rm S}_0, I m_{\rm I}|D|\gamma, J = 1, F m_{\rm F}\rangle A = \sum_{m_{\rm I}+m_J=m_{\rm F}}^{\gamma} C^{F}_{m_J m_{\rm I}} \langle {}^1{\rm S}_0 I m_{\rm I}|D|\gamma, m_{\rm I} m_J\rangle A, \tag{A.2}$$

where

$$A \equiv \frac{\langle \gamma, J, F m_{\rm F}|V_{\rm hf}|{}^3{\rm P}_0, F m_{\rm F}\rangle}{E(\gamma) - E({}^3{\rm P}_0)},$$

and $C^{F}_{m_J m_I}$ is the Clebsch–Gordon coefficient for the state $|\gamma, J = 1, F\rangle$.

For the convenience of discussion, we now consider the concrete example of ^{171}Yb, which has a nuclear spin of $I = 1/2$. It is obvious that the matrix element is nonzero for both the π-polarized laser field and the circularly polarized laser field. For π-polarized lasers, the matrix element is effectively given by

$$\langle \gamma, J = 1, m_J = 0, m_{\rm I} = \pm\tfrac{1}{2}|D|{}^1{\rm S}_0, m_J = 0, m_{\rm I} = \pm\tfrac{1}{2}\rangle; \tag{A.3}$$

whereas for circularly polarized lasers, the matrix element is effectively given by

$$\langle \gamma, J = 1, m_J = \pm 1, m_{\rm I} = \mp\tfrac{1}{2}|D|{}^1{\rm S}_0, m_J = 0, m_{\rm I} = \mp\tfrac{1}{2}\rangle, \tag{A.4}$$

for σ^+- and σ^--polarized light, respectively.

The ratio between the matrix elements in the two cases is given by that of the corresponding Clebsch–Gordon coefficients in equation (A.2). One may further relate these matrix elements to the natural linewidth Γ of the clock transition:

$$|\langle D\rangle|^2 = \frac{3\pi\epsilon_0\hbar c^3}{\omega_0^3}\beta\Gamma, \tag{A.5}$$

where ω_0 is the frequency for the clock transition. The constant factor β comes from the Clebsch–Gordon coefficient, which has $\beta = 1/3$ for π-polarized lasers and $\beta = 2/3$ for circularly polarized lasers. For ^{171}Yb, $\Gamma \sim 2\pi \times 10$ mHz [27]–[29], and a typical laser intensity of $I = 10\,{\rm kW\,cm^{-2}}$ gives a Rabi frequency of $\sim 2\pi \times 220$ kHz for a circularly polarized field.

References

[1] Bloch I, Dalibard J and Zwerger W 2007 Many-body physics with ultracold gases *Preprint* 0704.3011v1

[2] Trotzky S, Cheinet P, Fölling S, Feld M, Schnorrberger U, Rey A M, Polkovnikov A, Demler E A, Lukin M D and Bloch I 2008 *Science* **319** 295

[3] Anderlini M, Lee P J, Brown B L, Sebby-Strabley J, Phillips W D and Porto J V 2007 *Nature* **448** 452

[4] Hein M, Dür W, Eisert J, Raussendorf R, Van den Nest M and Briegel H J 2006 *Proc. of the Int. School of Physics Enrico Fermi on Quantum Computers, Algorithms and Chaos (Varenna, Italy)* vol 162 ed P Zoller and G Casati p 115

[5] Loss D and DiVincenzo D P 1998 *Phys. Rev.* A **57** 120

[6] Deutsch I H and Jessen P S 1998 *Phys. Rev.* A **57** 1972
[7] Dutta S K, Teo B K and Raithel G 1999 *Phys. Rev. Lett.* **83** 1934
[8] Haycock D L, Alsing P M, Deutsch I D, Grondalski J and Jessen P S 2000 *Phys. Rev. Lett.* **85** 3365
[9] Görlitz A, Kinoshita T, Hänsch T W and Hemmerich A 2001 *Phys. Rev.* A **64** 011401
[10] Dubetsky B and Berman P R 2002 *Phys. Rev.* A **66** 045402
[11] Ritt G, Geckeler C, Salger T, Cennini G and Weitz M 2006 *Phys. Rev.* A **74** 063622
[12] Zhang R, Sapiro R E, Morrow N V and Raithel G 2006 *Phys. Rev.* A **74** 033403
[13] Ravaine B, Derevianko A and Berman P R 2006 *Phys. Rev.* A **74** 022330
[14] Salger T, Geckeler C, Kling S and Weitz M 2007 *Phys. Rev. Lett.* **99** 190405
[15] Arun R, Averbukh I Sh and Pfau T 2005 *Phys. Rev.* A **72** 023417
[16] Kazantsev A P, Surdutovich G I and Yakovlev V P 1990 *Mechanical Action of Light on Atoms* (Singapore: World Scientific)
[17] Grimm R, Söding J and Ovchinnikov Yu B 1995 *JETP Lett.* **61** 367
[18] Hofferberth S, Lesanovsky I, Fischer B, Verdu J and Schmiedmayer J 2006 *Nat. Phys.* **2** 710
[19] Takamoto M, Hong F L, Higashi R and Katori H 2005 *Nature* **435** 321
[20] Ludlow A D, Boyd M M, Zelevinsky T, Foreman S M, Blatt S, Notcutt M, Ido T and Ye J 2006 *Phys. Rev. Lett.* **96** 033003
[21] Fukuhara T, Takasu Y, Kumakura M and Takahashi Y 2007 *Phys. Rev. Lett.* **98** 030401
[22] Hayes D, Julienne P S and Deutsch I H 2007 *Phys. Rev. Lett.* **98** 070501
[23] Babcock N S, Stock R, Raizen M G and Sanders B C 2008 *Can. J. Phys.* **86** 549
[24] Büchler H P, Hermele M, Huber S D, Fisher M P and Zoller P 2005 *Phys. Rev. Lett.* **95** 040402
[25] Boyd M M, Ludlow A D, Blatt S, Foreman S M, Ido T, Zelevinsky T and Ye J 2007 *Phys. Rev. Lett.* **98** 083002
[26] Boyd M M 2007 *PhD Thesis* University of Colorado
[27] Hoyt C W, Barber Z W, Oates C W, Fortier T M, Diddams S A and Hollberg L 2005 *Phys. Rev. Lett.* **95** 083003
[28] Porsev S G, Derevianko A and Fortson E N 2004 *Phys. Rev.* A **69** 021403
[29] Porsev S G and Derevianko A 2004 *Phys. Rev.* A **69** 042506
[30] Santra R, Christ K V and Greene C H 2004 *Phys. Rev.* A **69** 042510
[31] Jaksch D, Briegel H J, Cirac J I, Gardiner C W and Zoller P 1999 *Phys. Rev. Lett.* **82** 1975
[32] Mandel O, Greiner M, Widera A, Rom T, Hänsch T W and Bloch I 2003 *Phys. Rev. Lett.* **91** 010407
[33] Ovsiannikov V D, Pal'chikov V G, Katori H and Takamoto M 2006 *Quantum Electron.* **36** 3
[34] Jaksch D, Bruder C, Cirac J I, Gardiner C W and Zoller P 1998 *Phys. Rev. Lett.* **81** 3108
[35] Gorshkov A V, Jiang L, Greiner M, Zoller P and Lukin M D 2008 *Phys. Rev. Lett.* **100** 093005
[36] Duan L M, Demler E and Lukin M D 2003 *Phys. Rev. Lett.* **91** 090402
[37] Burkard G, Loss D and DiVincenzo D P 1999 *Phys. Rev.* B **59** 2070
[38] Coleman S 1977 *Phys. Rev.* D **15** 2929
[39] Callan C G and Coleman S 1977 *Phys. Rev.* D **16** 1762
[40] Lundblad N, Lee P J, Spielman I B, Brown B L, Phillips W D and Porto J V 2008 *Phys. Rev. Lett.* **100** 150401
[41] Zhang C W, Rolston S L, Das Sarma S and Coleman S 2006 *Phys. Rev.* A **74** 042316
[42] Cho J 2007 *Phys. Rev. Lett.* **99** 020502
[43] Rey A M, Gritsev V, Bloch I, Demler E and Lukin M D 2007 *Phys. Rev. Lett.* **99** 140601